Controllable Electrochemical Synthesis of Ce4+−Doped ZnO Nanostructures from Nanotubes to Nanorods and Nanocages

ARTICLE *in* CRYSTAL GROWTH & DESIGN · MARCH 2008

Impact Factor: 4.89 · DOI: 10.1021/cg7009995

5 AUTHORS, INCLUDING:

Lu Hong
Beihang University(BUAA)
189 PUBLICATIONS **2,742** CITATIONS
SEE PROFILE

Yexiang Tong
Sun Yat-Sen University
297 PUBLICATIONS **9,276** CITATIONS
SEE PROFILE

CRYSTAL GROWTH & DESIGN
2008
VOL. 8, NO. 4
1276–1281

Controllable Electrochemical Synthesis of Ce^{4+}-Doped ZnO Nanostructures from Nanotubes to Nanorods and Nanocages

Gao-Ren Li,*[,†,‡] Xi-Hong Lu,[†] Wen-Xia Zhao,[§] Cheng-Yong Su,*[,†] and Ye-Xiang Tong*[,†]

MOE of Key Laboratory of Bioinorganic and Synthetic Chemistry, School of Chemistry and Chemical Engineering, Institute of Optoelectronic and Functional Composite Materials, Sun Yat-Sen University, Guangzhou 510275, China, State Key Lab of Rare Earth Materials Chemistry and Applications, Beijing 100871, China, Instrumental Analysis and Research Center, Sun Yat-Sen University, Guangzhou 510275, China

Received October 12, 2007; Revised Manuscript Received February 17, 2008

ABSTRACT: The controllable electrochemical synthesis of Ce^{4+}-doped ZnO nanostructures from nanotubes to nanorods and nanocages is reported. The electrochemical route for the preparation of Ce^{4+}-doped ZnO nanostructures represents a simple, quick, and economical method. The growth mechanisms for Ce^{4+}-doped ZnO nanotubes, nanorods, and nanocages are proposed here. Ce^{4+}-doped ZnO nanotubes and nanocages formed when the crystal growth was only proceeded on the sides of six $(10\bar{1}0)$ facets of a hexagonal planar nucleus with preferential growth in the (0001) direction. The hexagonal Ce^{4+}-doped ZnO nanorods were formed when the crystal growth proceeded on the whole hexagonal planar nucleus with preferential growth in the (0001) direction. The X-ray diffraction, energy dispersive spectroscopy, X-ray photoelectron spectroscopy, transmission electron microscopy, high-resolution transmission electron microscopy, and selected area electron diffraction were used to characterize the phase, composition, and qualities of the prepared Ce^{4+}-doped ZnO nanotubes, nanorods, and nanocages. In addition, the photoluminescence properties of the prepared Ce^{4+}-doped ZnO nanotubes, nanorods, and nanocages were investigated.

1. Introduction

It is well-known that because of the quantum size effect and the high surface to volume ratio the reduction of microstructure sized crystalline materials into nanometer size can result in a dramatic modification of their magnetic, electronic, and optical properties.[1] In recent years, one-dimensional (1D) nanostructures, such as nanorods, nanowires, nanobelts, and nanotubes, have attracted intense attention due to their potential applications in a variety of novel nanodevices, such as field-effect transistors,[2] single-electron transistors,[3] photodiodes,[4,5] and chemical sensors.[6,7] Considerable efforts have been spent on the synthesis of these nanostructures, and various approaches have been reported. The electrodeposition route was widely used to prepare 1D nanostructures by the aid of anodic aluminum oxide (AAO) that endows access to uniform and distinct morphologies in large scales with remarkable reliability. However, this process is very troublesome, involving AAO fabrication and removal of the AAO template. Recently, the electrochemical assembly synthesis of 1D nanostructures without any template has attracted much attention, which represents a simple, quick, and economical method.

As an important low-cost basic II−VI functional semiconductor material, zinc oxide (ZnO) has attracted much research interest in both fundamental research and practical studies because of its excellent catalytic, optical, electrical, optoelectronic, gas-sensing, piezoelectric, and photoelectrochemical properties.[8,9] However, for practical device applications, the proper dopants may be introduced into ZnO, and the optical, electronic, and magnetic properties of ZnO can be greatly influenced by the chemical doping or formed intrinsic lattice defects.[10] For example, the transition-metal (such as, Fe, Ni, Co, Mn, Cr, V) doped ZnO is a potential diluted magnetic semiconductor that can provide efficient injection of spin-polarized carriers for spintronic devices. The optical/electrical properties of ZnO can be remarkably enhanced by doping Pb, Sn, Al, Ga, and Sb. Recently, much attention has been paid to rare-earth (RE) doped ZnO for possible applications in visible emitting phosphors in displays, high power lasers, and other optoelectronic devices.[11–19] Since CeO_2 has a band gap of about 3 eV and shows interesting optical properties such as optical transparency and strong UV absorption that are similar to that of ZnO,[20,21] the mixed CeO_2−ZnO have been investigated for the searching of highly efficient catalysts or UV filters.[22–27]

So far, various synthesis methods of RE-doped ZnO nanostructures have been reported, including the hydrothermal method,[15] magnetron sputter deposition,[12] pulsed laser deposition,[21] and photolithography and wet chemical etching.[16] In this paper, we report an electrochemical route for the selective synthesis of Ce^{4+}-doped ZnO nanotubes, nanorods, and nanocages without any template, offering an effective method to control the nanostructural morphology and size by adjusting current density, additive reagent, and salt concentration. Furthermore, this electrochemical synthesis route provides a simple and economical preparation for large area of Ce^{4+}-doped ZnO nanotubes, nanorods, and nanocages. To the best of our knowledge, this is the first report on the preparation of Ce^{4+}-doped ZnO nanotubes, nanorods, and nanocages by an electrochemical self-assembly route without any template.

2. Experimental Procedures

The dehydrated $Ce(NO_3)_3$ was obtained by the reaction of Ce_2O_3 (99.99 wt%) with HNO_3 and H_2O_2, and then dehydrating in a vacuum at 353 K. A simple three-electrode cell was used in our experiments. Electrochemical deposition was carried out in solution of $Ce(NO_3)_3$ and $Zn(NO_3)_2$ via galvanostatic electrolysis. The working electrodes were copper (99.99 wt%) with surface area of 0.8 cm^2. A graphite rod (spectral grade, 2.0 cm^2) was used as the counter-electrode. A saturated calomel electrode (SCE) was used as the reference electrode that was

* To whom correspondence should be addressed. E-mail: ligaoren@mail.sysu.edu.cn (G.-R.L.); cesscy@mail.sysu.edu.cn (C.-Y.S.); chedhx@mail.sysu.edu.cn (Y.-X.T.).
† Institute of Optoelectronic and Functional Composite Materials, Sun Yat-Sen University.
‡ State Key Lab of Rare Earth Materials Chemistry and Applications.
§ Instrumental Analysis and Research Center, Sun Yat-Sen University.

10.1021/cg7009995 CCC: $40.75
Published on Web 03/05/2008

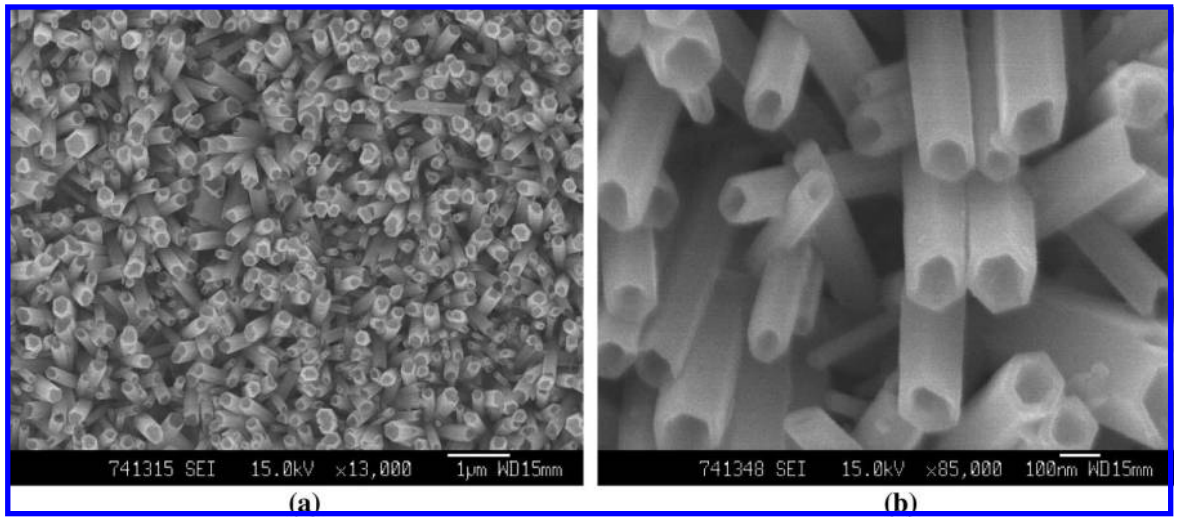

Figure 1. SEM images of Ce^{4+}-doped ZnO nanotubes prepared in solution of 0.01 M $Zn(NO_3)_2$ + 0.01 M $Ce(NO_3)_3$ + 0.01 M CH_3COONH_4 with a current density of 1 mA/cm^2 for 90 min at 70 °C. (a) ×13000; (b) ×85000.

connected to the cell with a double salt bridge system. All potential values determined in this study were the values versus SCE. The microstructures of deposits were characterized by field emission scanning electron microscopy (FE-SEM; JSM-6330F) and transmission electron microscopy (TEM; JEM-2010HR). The high-resolution transmission electron microscopy (HRTEM) images and the selected area electron diffraction (SAED) patterns were also recorded. The compositions and structures of deposits were analyzed by X-ray energy dispersive spectroscopy (EDS) and X-ray diffraction (XRD), respectively.

3. Results and Discussion

The electrochemical deposition was carried out in solution of 0.01 M $Zn(NO_3)_3$ + 0.01 M $Ce(NO_3)_3$ + 0.01 M CH_3COONH_4 with a current density of 1.0 mA cm^{-2} for 90 min at 70 °C. The high density Ce^{4+}-doped ZnO nanotubes were successfully prepared on a large area of Cu substrate, and their SEM images are shown in Figure 1. The diameters of these nanotubes are about 100 nm, and the thicknesses of the walls are about 10 nm. The lengths of Ce^{4+}-doped ZnO nanotubes are about 1 μm. Ce^{4+}-doped ZnO formation process is suggested as follows. First, NO_3^- ions are electroreduced on the cathode surface, and OH^- ions will be formed. Then the produced OH^- ions will react with Ce^{3+} and O_2 in deposition solution to form CeO_2. These processes can be expressed as eqs 1 and 2.[28]

$$NO_3^- + H_2O + 2e \rightarrow NO_2^- + 2OH^- \quad (1)$$

$$4Ce^{3+} + 12OH^- + O_2 \rightarrow 4CeO_2 + 6H_2O \quad (2)$$

With increasing concentration of OH^-, $Zn(OH)_4^{2-}$ will form. Then the produced $Zn(OH)_4^{2-}$ will subsequently be decomposed to form ZnO at a temperature of 70 °C via eqs 3, 4, and 5.[29]

$$Zn^{2+} + 2OH^- \rightarrow Zn(OH)_2 \quad (3)$$

$$Zn(OH)_2 + 2OH^- \rightarrow Zn(OH)_4^{2-} \quad (4)$$

$$Zn(OH)_4^{2-} \rightarrow ZnO + H_2O + 2OH^- \quad (5)$$

Therefore, during electrodeposition the mixed ZnO and CeO_2 were always obtained, and accordingly the Ce^{4+}-doped ZnO deposits were formed.

To confirm the compositions of Ce^{4+}-doped ZnO, EDS measurement was carried out at a number of locations throughout the deposits. Figure 2 shows a representative EDS pattern of Ce^{4+}-doped ZnO, and it revealed the elements of O, Zn, and

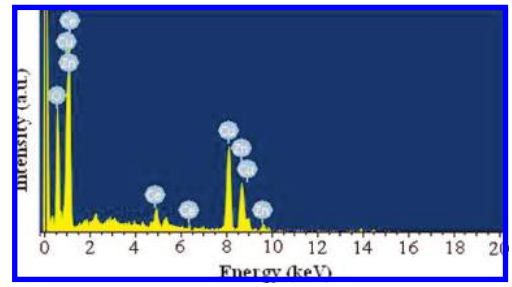

Figure 2. EDS spectrum of the prepared Ce^{4+}-doped ZnO deposits.

Ce existed in the obtained deposits. The Cu peaks come form the substrate. The composition analysis by EDS revealed Ce of about 3.4 at% incorporated into the ZnO lattice. Further evidence for the qualities and compositions of Ce^{4+}-doped ZnO compounds were obtained by XPS of deposits. The binding energies obtained in the XPS analysis were corrected for specimen charging by referencing the C 1s to 284.60 eV. The survey XPS spectrum of Ce^{4+}-doped ZnO shown in Figure 3a suggests that there are no other elements on the surface of the samples. The fine XPS spectrum of Zn $2p_{3/2}$ is displayed in Figure 3b, and the peak located at 1022 eV corresponds to Zn^{2+} species. The Ce $3d_{3/2}$ and $3d_{5/2}$ XPS spectra of deposit was shown in Figure 3c, which illustrates the presence of Ce^{4+} species on the surface of deposit. No Ce^{3+} species was detected. The O 1s spectrum for the surface of the sample demonstrates an O^{2-} peak at 531.30 eV as shown in Figure 3d. So the results of XPS further proved Ce^{4+}-doped ZnO compounds were obtained. The composition analysis by XPS revealed the content of Ce^{4+} in deposits was about 3.6 at %.

XRD measurement was performed to probe the crystal structure and phase purity of the prepared Ce^{4+}-doped ZnO deposits, and the XRD pattern of Ce^{4+}-doped ZnO deposit was shown in Figure 4. Three peaks at about 31.75, 34.43, and 36.25 degrees can be indexed to (100), (002), and (101) of wurtzite-structured ZnO (JCPDS card 36-1451). No Ce, CeO_2, or Ce_2O_3 peak is detected besides Cu peaks that come from the substrate. Therefore, the wurtzite is the only phase in existence in deposits, which indicates the possible uniform doping throughout the deposits. In addition, it should be noted that a lower angle shift was observed for the peaks of the prepared Ce^{4+}-doped ZnO deposits in XRD patterns relative to that of pure ZnO, which

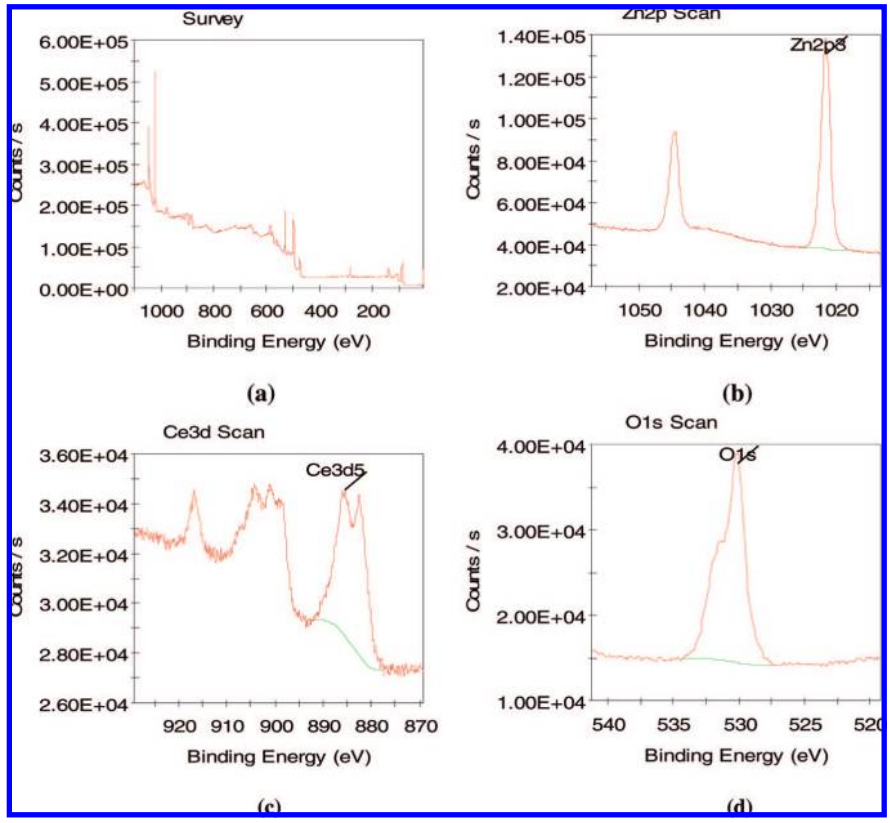

Figure 3. XPS analysis of the prepared Ce^{4+}-doped ZnO. (a) Survey scan, and high resolution scans of (b) Zn region, (c) Ce region, and (d) O region.

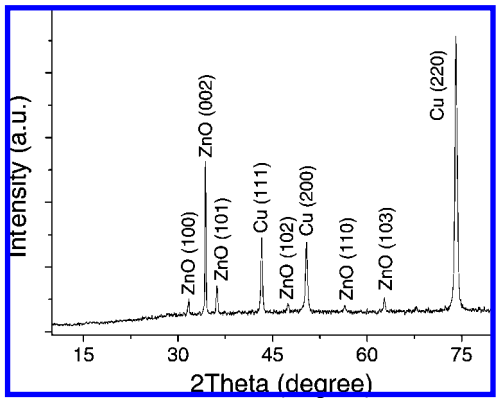

Figure 4. XRD pattern of Ce^{4+}-doped ZnO prepared in a solution of 0.01 M $Zn(NO_3)_2$ + 0.01 M $Ce(NO_3)_3$ + 0.01 M CH_3COONH_4 with current density of 1 mA/cm^2 for 90 min at 70 °C.

indicates Ce^{4+} ions have been doped into ZnO lattice. The lower angle shift of peaks of Ce^{4+}-doped ZnO deposits can be explained as follows. The ionic radius of the tetrahedrally coordinated Zn^{2+} is 0.74 Å, and that of the Ce^{4+} is 1.01 Å. When Ce^{4+} ions were incorporated into ZnO, the lattice parameters will be slightly increased, which will cause shifts of ZnO (100), (002), and (101) peaks to lower angles. Because of the resolution limit of XRD, the existence of CeO_2 phase possibly cannot be completely excluded even though no other secondary phases were observed in XRD. Therefore, the measurement of HRTEM was carried out to further examine the microstructure of Ce^{4+}-doped ZnO deposits. The TEM image in Figure 5a shows the obtained Ce^{4+}-doped ZnO deposits were tube-like structures. The HRTEM image for the prepared Ce^{4+}-doped ZnO nanotube was shown in Figure 5b, which clearly shows that the lattice fringes derive from the same crystalline grains. The lattice spacing estimated from the HRTEM image was found to be around 0.26 nm, which corresponds to the (0002) planar spacing of ZnO in the wurtzite phase. So the crystal growth of the nanotubes is preferential in the [0001] direction. The prepared Ce^{4+}-doped ZnO nanotubes was further characterized by SAED. The SAED pattern was shown in the inset in Figure 5c, and it also shows that the prepared Ce^{4+}-doped ZnO nanotube consists of single crystal structures with preferential growth in the [0001] direction. Therefore, the uniformly Ce^{4+}-doped ZnO nanotubes were successfully obtained.

However, when the current density of electrodeposition was increased to 1.5 mA/cm^2, the surface morphologies of deposits were changed from nanotubes to nanorods as shown in Figure 6. The diameters of these nanorods are about 60−100 nm, and the lengths are about 1 μm. The TEM, HRTEM, and SAED of the prepared Ce^{4+}-doped ZnO nanorods were also preformed, and their images are shown in Figure 7. The HRTEM image and SAED pattern both show the Ce^{4+}-doped ZnO nanotube consists of single crystal structures. The lattice spacing in the HRTEM image was calculated to be about 0.26 nm, which corresponds to the (0002) planar spacing of ZnO in the wurtzite phase. So the crystal growth of the nanorods is also preferential in the [0001] direction. When the additive CH_3COONH_4 was changed to KNO_3, namely, the electrochemical deposition of Ce^{4+}-doped ZnO was carried out in solution of 0.01 M $Zn(NO_3)_2$ + 0.01 M $Ce(NO_3)_3$ + 0.2 M KNO_3 with a current density of 4 mA cm^{-2} for 45 min at 90 °C. The Ce^{4+}-doped ZnO nanocages that are half-hollow structures were obtained on a large area of Cu substrate as shown in Figure 8. The sizes of these nanocages are about 200 nm. The deepness of hollow structures of these nanocages is about 100 nm. In addition, it

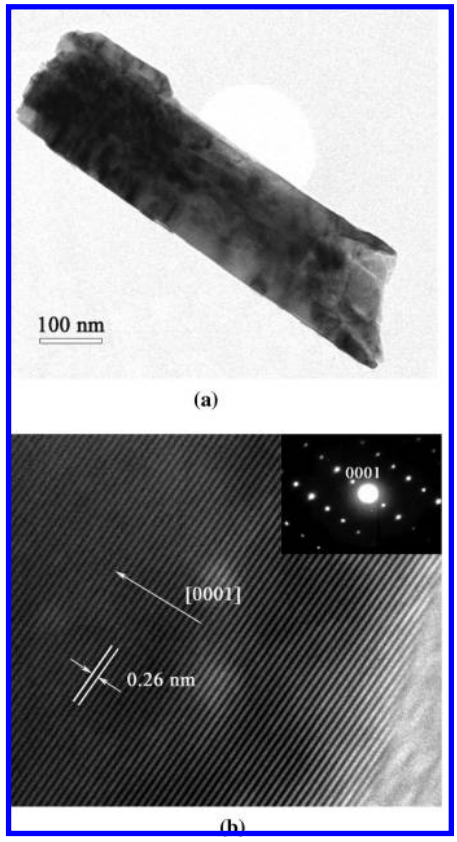

Figure 5. TEM image (a), HRTEM image (b), and SAED pattern (inset) of the prepared Ce^{4+}-doped ZnO nanotubes.

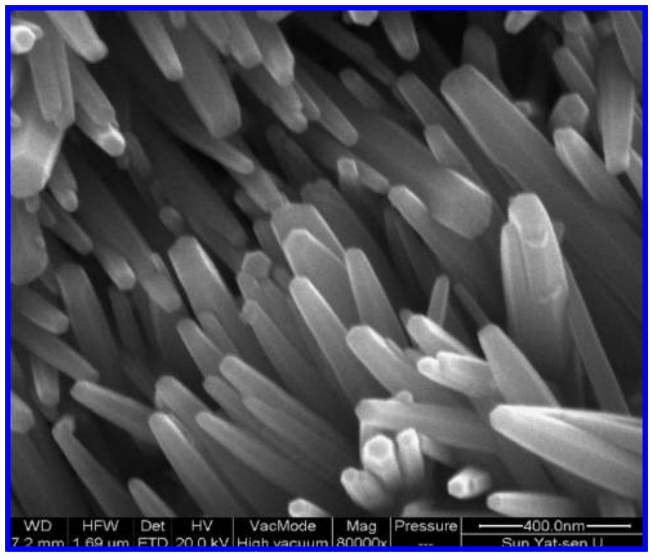

Figure 6. SEM image of Ce^{4+}-doped ZnO nanorods prepared in a solution of 0.01 M $Zn(NO_3)_2$ + 0.01 M $Ce(NO_3)_3$ + 0.01 M CH_3COONH_4 with a current density of 1.5 mA/cm^2 for 90 min at 70 °C.

should be noted that the profiles of these nanocages almost are similar to the hexagons as shown in the inset in Figure 8, and the length of every side of the hexagon is about 100 nm.

A schematic illustration for the growths of Ce^{4+}-doped ZnO nanotubes, nanorods, and nanocages during electrodeposition is shown in Figure 9. Since the Ce^{4+} ions were doped into ZnO lattices, the crystal structures of the doped deposits were determined by ZnO phase. As discussed above, the HRTEM

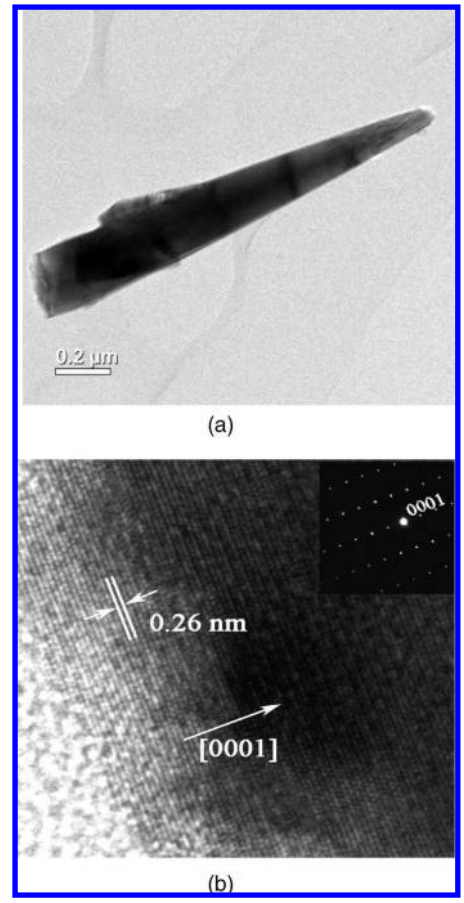

Figure 7. TEM image (a), HRTEM image (b), and SAED pattern (inset) of the prepared Ce^{4+}-doped ZnO nanorods.

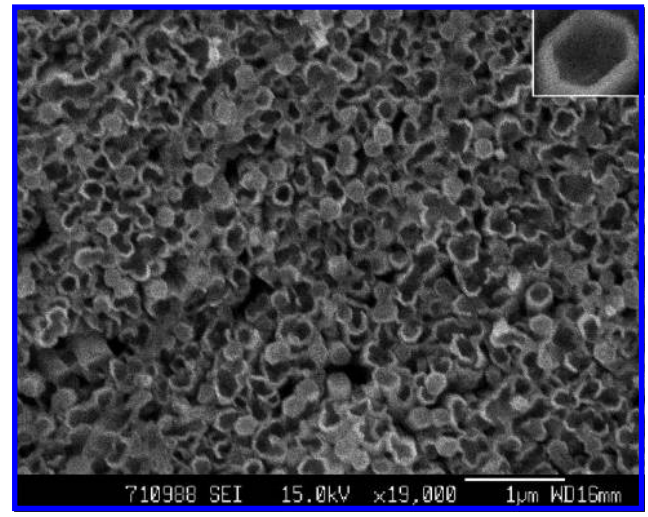

Figure 8. SEM image of Ce^{4+}-doped nanocages prepared in a solution of 0.01 M $Zn(NO_3)_2$ + 0.01 M $Ce(NO_3)_3$ + 0.2 M KNO_3 with current density of 4 mA/cm^2 for 45 min at 90 °C.

images and SAED patterns all confirmed that the Ce^{4+}-doped ZnO deposits had the same structures as the single crystal ZnO. During electrodeposition, these deposited Ce^{4+}-doped ZnO species first form seeds, and then these seeds grow in dimension to form a hexagonal ZnO planar nucleus. There are two polar surfaces (0001) and six side facets ($10\bar{1}0$) for the hexagonal wurtzite ZnO. When the current density is relative low, the electrochemical deposition rate was slow, same as the ion

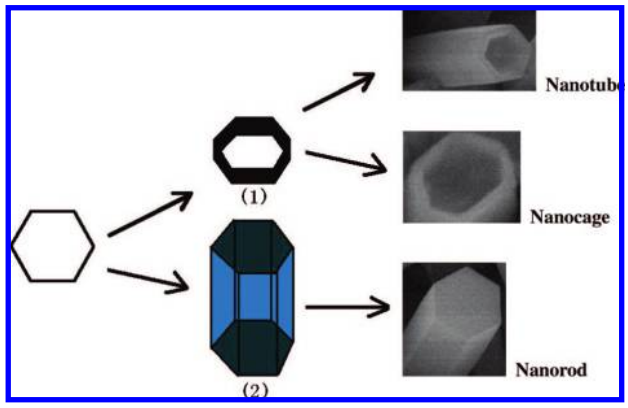

Figure 9. The schematic illustration for the growth of Ce^{4+}-doped ZnO nanotube, nanocage, and nanorod during electrodeposition.

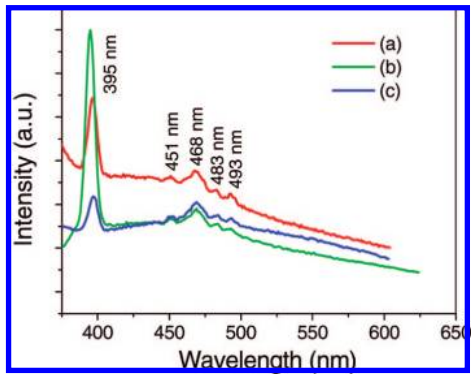

Figure 10. PL spectra of the prepared Ce^{4+}-doped ZnO deposits. (a) Nanotubes; (b) nanorods; (c) nanocages.

transfer speed. This will lead to the crystal growth easily happening on the sides of six $(10\bar{1}0)$ facets, and the crystal growth in the central section will become very difficult because these ions have been deposited on the sides before they were transferred to the central section. Under this situation, Ce^{4+}-doped ZnO nanotubes or nanocages will be formed since the crystal growth only proceeded on the sides of six $(10\bar{1}0)$ facets of the hexagonal planar nucleus with preferential growth in the (0001) direction as depicted in Figure 9(1). However, when the current density is relative high, the electrochemical deposition rate is fast, and the ion transfer becomes faster and can be easily transferred to the central section. This will lead to the formation of the hexagonal Ce^{4+}-doped ZnO nanorods because the crystal growth proceeds on the whole hexagonal planar nucleus with preferential growth in the (0001) direction as depicted in Figure 9(2).

Photoluminescence (PL) properties of these prepared various Ce^{4+}-doped ZnO nanostructures were investigated. Figure 9a−c shows room temperature PL spectra of nanotubes, nanorods, and nanocages, respectively. Normally, the pure bulk ZnO mainly exhibits a narrow emission peak near the band-edge free-exciton emission at about 390 nm and a broad deep-level emission around 460 nm, and the full width at half-maximum (fwhm) of the UV emission is about 18 nm.[30] In above various Ce^{4+}-doped ZnO nanostructures, the dominant UV emission bands are centered at about 395 nm and ascribed to the free recombination of excitons corresponding to the band edge emission of ZnO. The fwhm of the UV emissions of the obtained Ce^{4+}-doped ZnO nanotubes, nanorods, and nanocages is calculated approximately to be 7.5 nm, 8.5 nm, and 8.0 nm, respectively. Therefore, their fwhm are much narrower than that of commercial ZnO bulk crystals, indicating that the obtained Ce^{4+}-doped ZnO nanostructures have a higher optical property. The difference of the emission intensity may relate to their different nanostructural morphology and crystallinity. On the contrary, the emissions in the visible region are weak and show structural peaks at 451, 468, 483, and 493 nm, obviously different from that of undoped ZnO nanostructures.[31] It is well-known that the undoped ZnO nanostructures usually display broad green light emission bands at about 500 nm originated from the electron–hole recombination at the defect sites due to electron transition from the shallow donor level of the intrinsic defect centers, such as interstitial zinc (Zn_i) and oxygen vacancy (V_O), to the valence band. When Ce^{4+} as activation ions are doped in ZnO matrix, the band gap of the host materials may be slightly altered, which may change the luminescent processes of the host materials. The Ce^{4+} ion has a strong tendency to attract electrons to show charge transfer transition, and, once an electron is trapped to convert Ce^{4+} to Ce^{3+} ion, transitions between 5d and 4f orbitals become possible which are subject to the subtle influence of the ZnO host matrix. Therefore, the band gap structure of ZnO nanostructures can be modulated substantially by dopped Ce^{4+} ions, which may account for multiemission peaks appearing at the blue-green region as shown in Figure 9. The above various optical properties between Ce^{4+}-doped ZnO nanotubes, nanorods, and nanocages correspond to the different nanostructures. Therefore, these results indicate that one could adjust the optical quality as well as the surface morphologies of the Ce^{4+}-doped ZnO nanostructures by changing deposition parameters or adding appropriate additives in the deposition solution.

4. Conclusions

In summary, the various Ce^{4+}-doped ZnO nanostructures including nanotubes, nanorods, and nanocages can be selectively synthesized by electrochemical deposition, which represents a simple, quick, and economical method. The results of XRD, EDS, XPS, HRTEM, and SAED revealed that the prepared Ce^{4+}-doped ZnO deposits are composed of single crystal structures with preferential growth in the (0001) direction. The PL spectra indicate that the Ce^{4+}-doped ZnO has a high optical property and is a kind of interesting PL material that shows multiemission peaks at the blue-green region. Moreover, this direct electrochemical synthetic method represents a considerable improvement for the preparation of adulterated ZnO samples because of it allows better control over their nanostructures and may therefore provide a better experimental basis for understanding and ultimately controlling the optoelectronic properties of this class of materials.

Acknowledgment. We acknowledge that this work was supported by the Natural Science Foundations of China (Grant Nos. 20603048 and 20573136), the Natural Science Foundations of Guangdong Province (Grant Nos. 06300070, 06023099, and 04205405), and the Foundations of Potentially Important Natural Science Research and Young Teacher Starting-up Research of Sun Yat-Sen University.

Note Added after ASAP Publication. This article was released ASAP on March 5, 2008. Equation 5 has been modified. The corrected version posted on March 14, 2008.

References

(1) Elssfah, E.; Tang, C. *J. Phys. Chem. C* **2007**, *111*, 8176–8179.
(2) Chung, S.-W.; Yu, J.-Y.; Heath, J. R. *Appl. Phys. Lett.* **2000**, *76*, 2068–2070.

(3) Notargiacomo, A.; Di Gaspare, L.; Scappucci, G.; Mariottini, G.; Giovine, E.; Leoni, R.; Evangelisti, F. *Mater. Sci. Eng., C* **2003**, *23*, 671–673.
(4) Hayden, O.; Agarwal, R.; Lieber, C. M. *Nat. Mater.* **2006**, *5*, 352–356.
(5) Feng, P.; Zhang, J. Y.; Li, Q. H.; Wang, T. H. *Appl. Phys. Lett.* **2006**, *88*, 153107–153110.
(6) Li, C.; Zhang, D.; Liu, X.; Han, S.; Tang, T.; Han, J.; Zhou, C. *Appl. Phys. Lett.* **2003**, *82*, 1613–1615.
(7) Kolmakov, A.; Zhang, Y.; Cheng, G.; Moskovits, M. *Adv. Mater.* **2003**, *15*, 997–1000.
(8) Yao, K. X.; Zeng, H. C. *J. Phys. Chem. B* **2006**, *110*, 14736–14743.
(9) Wang, Z. L.; Song, J. H. *Science* **2006**, *312*, 242–246.
(10) (a) Deng, R.; Zhang, X. T.; Zhang, E.; Liang, Y.; Liu, Z.; Xu, H.; Hark, S. K. *J. Phys. Chem. C* **2007**, *111*, 13013–13015. (b) Fujihara, S.; Ogawa, Y.; Kasai, A. *Chem. Mater.* **2004**, *16*, 2965–2968. (c) Chu, D.; Zeng, Y.-P.; Jiang, D. *J. Phys. Chem. C* **2007**, *111*, 5893–5897. (d) Deng, R.; Zhang, X.; Zhang, E.; Liang, Y.; Liu, Z.; Xu, H.; Hark, S. *J. Phys. Chem. C* **2007**, *111*, 13013–13015. (e) Meron, T.; Markovich, G. *J. Phys. Chem. B* **2005**, *109*, 20232–20236.
(11) John, J. S.; Coffer, J. L. *Appl. Phys. Lett.* **2000**, *77*, 1635–1637.
(12) Teng, X. M.; Fan, H. T.; Pan, S. S.; Ye, C.; Li, G. H. *J. Appl. Phys.* **2006**, *100*, 053507.
(13) Duclère, J.-R.; Doggett, B.; Henry, M. O.; McGlynn, E.; Rajendra Kumar, R. T.; Mosnier, J.-P. *J. Appl. Phys.* **2007**, *101*, 013509.
(14) Wang, J.; Zhou, M. J.; Hark, S. K.; Li, Q.; Tang, D.; Chu, M. W.; Chen, C. H. *Appl. Phys. Lett.* **2006**, *89*, 221917.
(15) Gao, S.; Zhang, H.; Deng, R.; Wang, X.; Sun, D.; Zheng, G. *Appl. Phys. Lett.* **2006**, *89*, 123125.
(16) Bhosle, V.; Tiwari, A.; Narayan, J. *J. Appl. Phys.* **2006**, *100*, 033713.
(17) Potzger, K.; Zhou, S.; Eichhorn, F.; Helm, M.; Skorupa, W.; Mücklich, A.; Fassbender, J.; Herrmannsdörfer, T.; Bianchi, A. *J. Appl. Phys.* **2006**, *99*, 063906.
(18) Cheng, B.; Xiao, Y.; Wu, G.; Zhang, L. *Adv. Funct. Mater.* **2004**, *14*, 913–919.
(19) Duclère, J.-R.; Doggett, B.; Henry, M. O.; McGlynn, E.; Rajendra Kumar, R. T.; Mosnier, J.-P.; Perrin, A.; Guilloux-Viry, M. *J. Appl. Phys.* **2007**, *101*, 013509.
(20) Chariditis, C.; Patsalas, P.; Logothetidis, S. *J. Phys.: Conf. Ser.* **2005**, *10*, 226.
(21) Mishra, B. G.; Rao, G. R. *Bull. Mater. Sci.* **2002**, *25*, 155–162.
(22) He, Y. J.; Yang, B. L.; Cheng, G. X. *Catal. Today* **2004**, *98*, 595–600.
(23) Mo, L. Y.; Zheng, X. M.; Yeh, C. T. *ChemPhysChem* **2005**, *6*, 1470–1472.
(24) He, Y. J.; Yu, X. Y.; Li, T. L.; Yan, L. Y.; Yang, B. L. *Powder. Technol.* **2006**, *166*, 72–76.
(25) Li, R. X.; Yabe, S.; Yamashita, M.; Momose, S.; Yoshida, S.; Yin, S.; Sato, T. *Solid State Ion.* **2002**, *151*, 235–241.
(26) Peverari, C.; Pires, A. M.; Gonçalves, R. R.; Serra, O. A. *Ecletica Quim.* **2005**, *30*, 59.
(27) Zhang, Z.; Liu, S.; Chow, S.; Han, M.-Y. *Langmuir* **2006**, *22*, 6335–6340.
(28) Li, G.-R.; Qu, D.-L.; Tong, Y.-X. *Electrochem. Commun.* **2008**, *10*, 80–84.
(29) (a) Peulon, S.; Lincot, D. *Adv. Mater.* **1996**, *8*, 166–170. (b) Izaki, M. *Appl. Phys. Lett.* **1996**, *68*, 2439.
(30) Song, R.-Q.; Xu, A.-W.; Deng, B.; Li, Q.; Chen, G.-Y. *Adv. Funct. Mater.* **2007**, *17*, 296–306.
(31) Li, G.-R.; Dawa, C.-R.; Bu, Q.; Lu, X.-H.; Ke, Z.-H.; Hong, H.-E.; Zheng, F.-L.; Yao, C.-Z.; Liu, G.-K.; Tong, Y.-X. *J. Phys. Chem. C* **2007**, *111*, 1919–1923.

CG7009995